

## METHODS

**Synthesis.** All in-plane lateral heterostructures were synthesized by water-assisted thermal evaporation from solid sources at atmospheric pressure, in a chemical vapour deposition system developed in-house. Bulk powders of MoSe<sub>2</sub> (99.9%, Sigma-Aldrich), WSe<sub>2</sub> (99.9%, Sigma-Aldrich) MoS<sub>2</sub> (99.9%, Sigma-Aldrich) or WS<sub>2</sub> (99.9%, Sigma-Aldrich) were used directly in different combinations for the synthesis of, mainly, four types of heterostructures: MoSe<sub>2</sub>-WSe<sub>2</sub> (150 mg); MoS<sub>2</sub>-WS<sub>2</sub> (150 mg); MoSe<sub>0.96</sub>S<sub>1.04</sub>-WSe<sub>0.92</sub>S<sub>1.08</sub> (MoSe<sub>2</sub>-WS<sub>2</sub> (150 mg)); MoS<sub>0.64</sub>Se<sub>1.36</sub>-WSe<sub>1.32</sub>S<sub>0.68</sub> (MoS<sub>2</sub>-WSe<sub>2</sub> (150 mg)). For the growth of MoX<sub>2</sub>-WX<sub>2</sub> (where X = S, Se), powder sources containing MoX<sub>2</sub> and WX<sub>2</sub> in a ratio of 2:1 were placed side-by-side within an alumina boat (L × W × H: 70 × 14 × 10 mm) in the centre of a 1-inch diameter horizontal quartz tube furnace. Si substrates, with a 300 nm SiO<sub>2</sub> layer, were pre-cleaned with acetone, isopropanol and deionized water. During the growth, the substrates were placed downstream at temperatures between 810 and 700 °C, 6–10 cm away from the solid sources at 1,060 °C. Initially, the temperature of the furnace was slowly raised to 1,060 °C over 50 min with a constant flow of N<sub>2</sub> (200 standard cubic centimetres per minute, s.c.c.m.) and both substrates and sources were kept outside the furnace. When the temperature of the furnace reached greater than 1,040 °C, the solid precursor and the substrates were moved to their respective positions, by sliding the quartz tube into the furnace, and simultaneously water vapour was introduced in a controlled manner by diverting N<sub>2</sub> flow through a bubbler (Sigma-Aldrich) containing 2 ml of deionized water at room temperature. In order to switch the growth from Mo-rich to W-rich compounds, resulting in a lateral heterostructure, the N<sub>2</sub> + H<sub>2</sub>O vapour flux was rapidly replaced by a mixture of Ar + 5% H<sub>2</sub> (200 s.c.c.m.). Similar growth conditions were employed for the growth of heterostructures with other compositions. Once the desired heterostructure sequence was completed, the synthesis process was abruptly terminated by sliding the quartz tube containing both the precursor and substrates to a cooler zone, while keeping a 200 s.c.c.m. constant flow of Ar + H<sub>2</sub> (5%) until it cooled to room temperature.

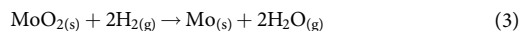
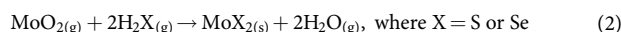
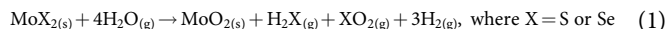
**Raman and photoluminescence spectroscopy.** The Raman and photoluminescence experiments were performed in a confocal microscope-based Raman spectrometer (LabRAM HR Evolution, Horiba Scientific) in backscattering geometry. Excitation wavelengths of 532 nm and 632 nm (laser power at the sample, 77 μW), focused with a 100× objective (numerical aperture 0.9, working distance 0.21 mm). During the photoluminescence and Raman mapping the optical path is stationary, while moving the sample on a computer controlled motorized XY stage.

**Transmission electron microscopy.** HAADF-STEM imaging was carried out on an aberration-corrected JEOL JEM-ARM200cF with a cold-field emission gun at 200 kV. The STEM resolution of the microscope is 0.78 Å. The HAADF-STEM images were collected with the JEOL HAADF detector using the following experimental conditions: probe size 7c, condenser lens aperture 30 μm, scan speed 32 μs per pixel, and camera length 8 cm, which corresponds to a probe convergence angle of 21 mrad and inner collection angle of 76 mrad.

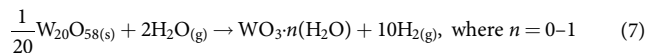
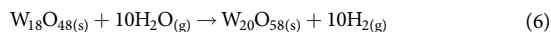
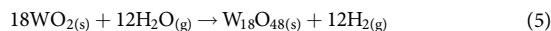
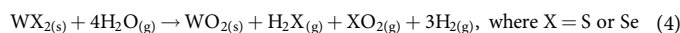
**Device fabrication.** To fabricate the electrical contacts to individual layers within MoX<sub>2</sub> and WX<sub>2</sub> domains, 80 nm of gold were deposited onto an 8 nm thick layer of titanium via e-beam evaporation. Contacts were patterned using standard e-beam lithography techniques. After gold deposition, and in order to extract adsorbates, the samples were annealed under high vacuum for 24 h at 120 °C. In the case of WSe<sub>2</sub>-MoSe<sub>2</sub> heterojunctions, before deposition, approximately 30 nm of hexagonal boron nitride crystals (Momentive PolarTherm PT110) were mechanically exfoliated from larger crystals, and transferred onto the heterostructure using a similar technique to that described in ref. 8.

**Electrical characterization.** Electrical characterization experiments were performed using a source meter (Keithley 2612 A). The sourcemeter was controlled via Labtracer2, free software available at <https://www.tek.com/source-measure-units/2400-c-software/labtracer-28-unsupported>. For photocurrent measurements, a Coherent Sapphire 532-150 CW CDRH and Thorlabs DLS146-101S were used, with a continuous wavelength λ of 532 nm. Light was transmitted to the sample through a 10-μm single-mode optical-fibre with a mode field diameter of 10 μm. The size of the laser spot was also measured against a fine grid. An I<sub>0</sub> value of the order of 10<sup>-12</sup> A yields diode ideality factors ranging from approximately 3.2 to 4.5, while yielding reasonable values for the shunt resistance R<sub>s</sub>, that is between approximately 2.5 and 4.5 MΩ. We find that good fits are obtained when I<sub>0</sub> is allowed to decrease to values below the noise floor of the measurements, approaching at least 10<sup>-15</sup> A. This uncertainty in the value of I<sub>0</sub> has no effect on the values of f or R<sub>s</sub>. The diode-like electrical responses were fitted using the Shockley diode equation in the presence of a series resistor R<sub>s</sub> (ref. 8):  $I_{ds} = \frac{nV_T}{R_s} W_0 \left\{ \frac{I_0 R_s}{f V_T} \exp\left(\frac{V_{ds} + I_0 R_s}{f V_T}\right) \right\} - I_0$ , where V<sub>T</sub> is the thermal voltage at a temperature T, I<sub>0</sub> is the reverse bias current, f is the diode ideality factor (f = 1 for an ideal diode) and W<sub>0</sub>[x] is the Lambert function. The results of the electrical characterization experiments are shown in Fig. 4 in detail.

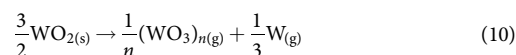
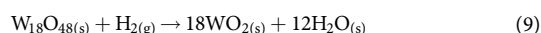
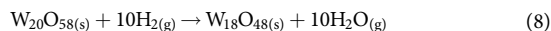
**Growth mechanism.** A preliminary study was performed to evaluate the interaction mechanism between water vapour and MoX<sub>2</sub> as well as WX<sub>2</sub> bulk powders. By allowing the solid precursor to interact with water vapour at 1,060 °C for a prolonged time (at least 20–30 min), it was found that different Mo (or W) oxide phases evolve, which are assumed to be the main driving force behind the selective growth of the individual compounds. It can be seen clearly from the Raman spectra (Extended Data Fig. 5a) that MoO<sub>2</sub> is the dominant phase evolving during the oxidation of MoS<sub>2</sub> or of MoSe<sub>2</sub>. The Raman peak position of the partially oxidized cluster shows the presence of both MoSe<sub>2</sub> (or MoS<sub>2</sub>) and MoO<sub>2</sub> phases, whereas from completely oxidized domains, only frequencies at 126, 203, 228, 347, 363, 458, 496, 570 and 742 cm<sup>-1</sup> were observed; this agrees well with the Raman spectra of MoO<sub>2</sub> (ref. 31). A previous report also confirmed that the main solid product during MoS<sub>2</sub> oxidation under water vapour at temperatures greater than 1,000 °C is MoO<sub>2</sub> (ref. 32) rather than MoO<sub>3</sub>, which tends to be a stable phase under various reactive gas environments<sup>33</sup>. Indeed, in our experiments, the overall oxidation reaction between MoX<sub>2</sub> and water at 1,060 °C led to the formation of MoO<sub>2</sub> (reaction (1)). Furthermore, it was found that the weight loss of Mo-oxides is very rapid in the presence H<sub>2</sub>O vapour (Extended Data Fig. 5c). Taking this into account, presumably, the sublimation of MoO<sub>2</sub> proceeds very rapidly at a temperature of 1,060 °C, and subsequently the vapour is transported and saturated on the desired substrate at relatively lower temperatures<sup>34</sup>. The recondensed MoO<sub>2</sub> vapour interacts with the H<sub>2</sub>X already present (as a by-product of oxidation) to form MoX<sub>2</sub> at temperatures ranging from 650 to 800 °C (reaction (2))<sup>34,35</sup>. This leads to the formation of MoX<sub>2</sub> domains. Notably, the growth of MoX<sub>2</sub> can be abruptly terminated by changing the carrier gas from wet nitrogen to dry argon with 5% hydrogen, which rapidly depletes the source of MoO<sub>2</sub> vapours owing to its reduction by hydrogen to metallic molybdenum at the surface of the source (reaction (3)). Unfortunately, the detection of the exact transport phases was not possible because of constrained access to the reaction tube of the chemical vapour deposition system under the conditions used for the growth of the TMD heterostructures. Therefore, only the most important reaction equations were derived:



By contrast, WX<sub>2</sub> has different oxidation and reduction behaviour (Extended Data Fig. 5c, d) under the above conditions, in which different W<sub>x</sub>O<sub>y</sub> oxide phases are observed in the Raman spectra (Extended Data Fig. 5b) and Supplementary Table 2. In the case of WSe<sub>2</sub>, distinct oxide phases evolved upon reaction with different reactive gas vapours for more than 20 min at 1,060 °C, as shown in Extended Data Fig. 5b<sup>36–38</sup>. The dominant phases observed in the Raman spectra are WO<sub>2</sub> (refs 36, 38, 39) and W<sub>20</sub>O<sub>58</sub> (ref. 37). This indicates that the oxidation state of W is dominated by that within WO<sub>2</sub> and W<sub>20</sub>O<sub>58</sub> during the oxidation reaction of WX<sub>2</sub> in wet nitrogen carrier gas by a series of reaction steps (reactions (4)–(7)):



The formation of any volatile WO<sub>3</sub>·(H<sub>2</sub>O) or similar tungstate species in N<sub>2</sub> + H<sub>2</sub>O vapour cannot be ruled out, however these species mostly condense below 500 °C<sup>40</sup> and hence might not be participating in the growth process. Similarly, in the presence of the reducing agent H<sub>2</sub>, the high-index W sub-oxides undergo a series of phase transformations to low-index oxide phases (reactions (8)–(10))<sup>34,41</sup>:



The different (WO<sub>3</sub>)<sub>n(g)</sub> species can be formed alongside the reduction process, and subsequently transported as vapour to the growth substrate (reaction (11)); the reaction of WO<sub>2</sub> is shown as reaction (12):